

Epitaxial mounding in limited mobility models of surface growth

P. Punyindu⁽¹⁾, Z Toroczkai^(1,2), and S. Das Sarma⁽¹⁾

⁽¹⁾ *Department of Physics, University of Maryland, College Park, MD 20742, USA*

⁽²⁾ *Theoretical Division and Center for Nonlinear Studies, Los Alamos National Laboratory, Los Alamos, New Mexico 87545, USA*

We study, through large scale stochastic simulations using the noise reduction technique, surface growth via vapor deposition e.g. molecular beam epitaxy (MBE), for simple nonequilibrium limited mobility solid-on-solid growth models, such as the Family (F) model, the Das Sarma-Tamborenea (DT) model, the Wolf-Villain (WV) model, the Larger Curvature (LC) model, and other related models. We find that $d=2+1$ dimensional surface growth in several noise reduced models (most notably the WV and the LC model) exhibits spectacular quasi-regular mound formation with slope selection in their dynamical surface morphology in contrast to the standard statistically scale invariant kinetically rough surface growth expected (and earlier reported in the literature) for such growth models. The mounding instability in these epitaxial growth models does not involve the Ehrlich-Schwoebel step edge diffusion barrier. The mounded morphology in these growth models arises from the interplay between the line tension along step edges in the plane parallel to the average surface and the suppression of noise and island nucleation. The line tension tends to stabilize some of the step orientations that coincide with in-plane high symmetry crystalline directions, and thus the mounds that are formed assume quasi-regular structures. The noise reduction technique developed originally for Eden type models can be used to control the stochastic noise and enhance diffusion along the step edge, which ultimately leads to the formation of quasi-regular mounds during growth. We show that by increasing the diffusion surface length together with suppression of nucleation and deposition noise, one can obtain a self-organization of the pyramids in quasi-regular patterns. The mounding instability in these simple epitaxial growth models is closely related to the cluster-edge diffusion (as opposed to step edge barrier) driven mounding in MBE growth, which has been recently discussed in the literature. The epitaxial mound formation studied here is a kinetic-topological instability (which can happen only in $d=2+1$ dimensional, or higher dimensional, growth, but *not* in $d=1+1$ dimensional growth because no cluster diffusion around a closed surface loop is possible in “one dimensional” surfaces), which is likely to be quite generic in real MBE-type surface growth. Our extensive numerical simulations produce mounded (and slope-selected) surface growth morphologies which are strikingly visually similar to many recently reported experimental MBE growth morphologies.

I. INTRODUCTION

Crystal growth, particularly high-quality epitaxial thin film growth, is one of the most fundamental processes impacting today’s technology [1]. A major issue in interface growth experiments is to have continuous dynamical control over the deposition process, such that interfaces with certain desired patterns can be obtained. For example, while in thin film epitaxy it is desirable to obtain smooth surfaces, in nanotechnology it is also important to be able to create regular, nanoscale structures with well defined geometry, such as quantum dots, quantum wires, etc. Growth is usually achieved by vapor deposition of atoms from a molecular beam (molecular beam epitaxy, or MBE). Thus, in order to be able to design a controlled deposition process, it is of crucial importance to understand *all* the instability types (which destroy controllability) that may occur during growth. In the present paper we concentrate on MBE growth. There are several types of instabilities in MBE among which we mention the Ehrlich-Schwoebel (ES) [2] instability which is of kinetic-energetic type. Ehrlich-Schwoebel (ES) barriers in the lattice potential induce an instability by hindering step-edge atoms on upper terraces from going down to lower terraces [2] which in turn can generate mounded structures during growth. The ES instability is thought to be an ubiquitous phenomenon in real surface deposition processes, and as such, is widely considered to be the only mechanism for formation of mounds in surface growth. Another kinetic-energetic instability, which does not involve any explicit ES barriers, was discussed by Amar and Family [3]. This instability involves a negative barrier at the base of a step, and thus is due to a short range *attraction* between adatoms and islands. Short range attractions generically lead to clustering in multiparticle systems, a property which in the language of MBE translates into formation of mounds. Note that this attraction-induced instability and ES instability are essentially equivalent, and both could occur in $d=1+1$ or $2+1$ dimensions. Both the attractive instability and the ES barrier instability cause mounding because atoms on terraces preferentially collect at up-steps rather than down-steps leading to the mounded morphology. In both cases, there is no explicit stabilizing mechanism, and the mounds should progressively stiffen with time leading to mounded growth morphology with no slope selection, where the mound slopes continue to increase as growth progresses. It is, of course, possible to stop the monotonic

slope increase by incorporating some additional mechanisms (e.g. the so-called “downward funneling” where deposited atoms funnel downwards before incorporation) which produce a downhill mass current on the surface and thereby opposes the uphill current created by the ES barrier. There is, however, no intrinsic slope selection process built in the ES barrier mechanism itself.

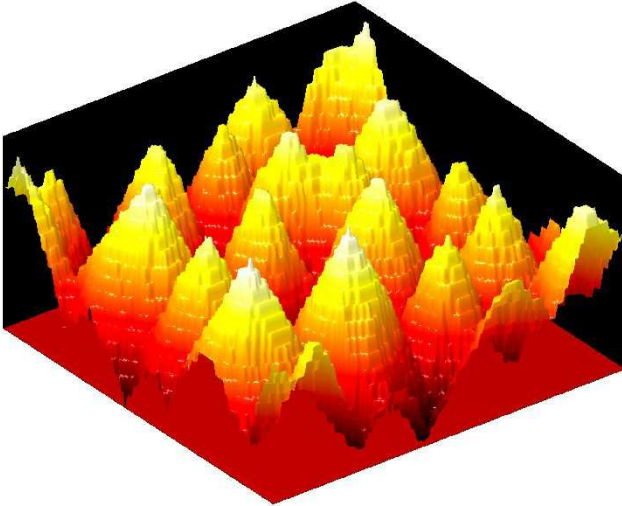


FIG. 1. Mounded morphology created by SED. This is a simulation of the LC model as described in the text.

The purpose of the current article is to discuss a completely different *kinetic-topological* mechanism, qualitatively distinct from the ES barrier induced mounding, which leads to spectacular mound formation (see Fig. 1 for a colorful example) in MBE growth without involving any ES barriers (or the closely related island-adatom attraction mechanism) whatsoever. Based on the direct stochastic numerical simulations of a large number of MBE-related nonequilibrium limited mobility solid-on-solid epitaxial growth models studied in this paper we believe that epitaxial mounding of the type discussed here is quite generic, and may actually apply to a variety of experimental situations where mounded growth morphologies (with slope selection) have been observed. The mechanism underlying the mounding instability discussed in this paper is closely related to that proposed in two recent publications [4,5] although its widespread applicability to well-known limited mobility MBE growth models, as described here, has not earlier been appreciated in the literature. The mounding instability discussed in this paper, being topological in nature, can happen only on physical two-dimensional surfaces ($d=2+1$ dimensions growth) or in (unphysical) higher ($d>2+1$) dimensional systems, in contrast to ES type instabilities which, being of energetic origin, are allowed in all dimensions.

The instability most recently discovered by Pierre-Louis, D’Orsogna, and Einstein [4], and independently by

Ramana Murty and Copper [5] is entirely different from ES instabilities, because it is *not* of kinetic-energetic nature (involving potential barriers) but rather of a *kinetic-topologic* nature. This instability is generated by strong diffusion along the edges of monoatomic steps, and its net effect in two or higher dimensions is to create quasi-regular shaped mounds on the substrate (see Fig. 1). For simplicity of formulation we will call this instability the step-edge diffusion, or SED instability. What comes as a bit of a surprise is that in spite of its simplicity as a mechanism, it has not apparently been recognized that the SED mechanism may actually be playing a dominant role in many epitaxial mounding instabilities. There are two reasons for this, one is probably because the ES instability has inadvertently and tacitly been accepted as the only mechanism for mounding, and therefore the mounded surface morphologies coming from experiments have been *apriori* analyzed with the ES mechanism in mind, and the second reason is that SED is not easy to see in simulations unless other conditions (related to reduced noise) are met in addition to the existence of edge-current, which we will discuss in details in the present paper.

In this paper we discuss the SED instability, and analyze its effects on various growth models, giving both a simple continuum and discrete description. The SED is shown to exist in a large number of discrete, limited mobility growth models, and we identify the conditions under which SED-induced epitaxial mounding is manifested. We study the instability by producing dynamical growth morphologies through direct numerical simulations and by analyzing the measured height-height correlation functions [6] of the simulated morphologies. This paper is organized as follows: in Section II we define a number of limited mobility growth models (Subsection II.A) studied here, we briefly review the noise reduction technique (Subsection II.B), then present a series of simulated growth morphologies, both from early and late times, with and without noise reduction (Subsection II.C); in Section III we describe and discuss the SED mechanism, by first presenting a continuum description in terms of local currents (Subsection III.A) and its discrete counterpart with particular emphasis on the Wolf-Villain and Das Sarma - Tamborenea models (Subsection III.B); in Subsection III.C we introduce the notion of conditional site occupation rates to analyze the effects of noise reduction; Section IV is devoted to the properties of the mounded morphologies with the emphasis on the relevance of the height-height correlation function (Subsection IV.A), where we note possible comparison with experiments and discuss the relevance of the global diffusion current in the simulations for the mounding instability.

II. MORPHOLOGIES OF DISCRETE LIMITED MOBILITY GROWTH MODELS

A. Models

All the models studied here are dynamical limited mobility growth models in which an adatom is allowed to diffuse (according to specific sets of diffusion rules for each model) within a finite diffusion length of l sites. The diffusion process is instantaneous and once the adatom has found its final site, it is incorporated permanently into the substrate and can no longer move. These models are also based on the solid-on-solid (SOS) constraint where bulk vacancies and overhangs are not allowed. Desorption from the growth front is neglected.

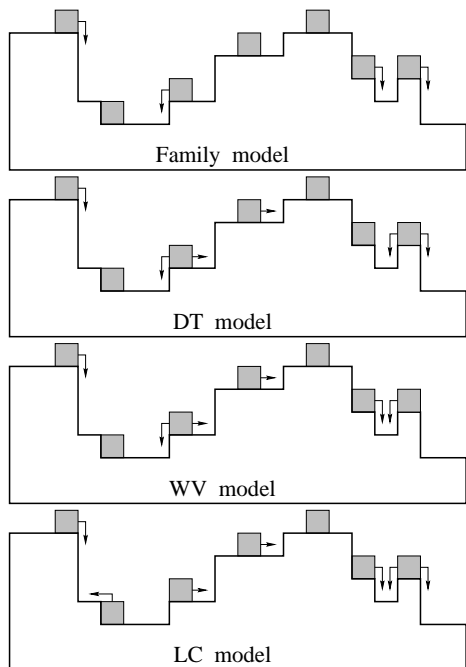


FIG. 2. Schematic configurations defining the diffusion growth rules in one dimension for various dynamical growth models discussed in this paper. Here $l = 1$.

With this SOS constraint, growth can be described on a coarse-grained level by the continuity equation

$$\frac{\partial h}{\partial t} + \nabla \cdot \mathbf{j} = F\Omega + \eta(\mathbf{x}, t), \quad (1)$$

where $h(\mathbf{x}, t)$ is the surface height measured in the growth direction, \mathbf{j} is the local (coarse-grained) surface diffusion current, F is the incoming particle flux, $\Omega = a_{\perp} a_{\parallel}^d$ is the surface cell volume with a_{\perp} and a_{\parallel} being the lattice constants in the growth direction and in the d -dimensional substrate, respectively. The shot noise is Gaussian uncorrelated white noise with correlator:

$$\langle \eta(\mathbf{x}, t) \eta(\mathbf{x}', t') \rangle = D \delta(\mathbf{x} - \mathbf{x}') \delta(t - t') \quad (2)$$

where the amplitude of the fluctuations D is directly proportional to the average incoming particle flux through the relation: $D = F\Omega^2$.

The most general form of this continuity equation [8] which preserves all the symmetries of the problem can be written as:

$$\frac{\partial h}{\partial t} = \nu_2 \nabla^2 h - \lambda_4 \nabla^4 h + \lambda_{22} \nabla^2 (\nabla h)^2 + \dots + \eta, \quad (3)$$

where h from now on indicates the height fluctuation around the average interface height $\langle h \rangle$. Note that the unit of time in our simulations is defined through $\langle h \rangle$; we arbitrarily choose the deposition rate of 1 monolayer (ML) per second, and all simulations are done with periodic boundary conditions along the substrate.

1. Family model

This is a model introduced by Family (F) [9] with the simplest diffusion rule: adatoms diffuse to the local height minima sites within range l (see the one dimensional version in Fig. 2). This is a well studied model and it is described on a coarse-grained level by the continuum Edwards-Wilkinson [10] equation $\frac{\partial h}{\partial t} = \nu \nabla^2 h + \eta$ and hence the model asymptotically belongs to the Edward-Wilkinson (EW) universality class.

2. Das Sarma-Tamborenea model

The Das Sarma-Tamborenea (DT) model was proposed [11] as a simple limited mobility nonequilibrium model for MBE growth. In this model, an adatom is randomly dropped on an initially flat substrate. If the adatom already has a coordination number of two or more (i.e. one from the neighbor beneath it to satisfy the SOS condition, and at least one lateral neighbor) at the original deposition site, it is incorporated at that site. If the adatom does not have a lateral nearest neighbor at the deposition site, it is allowed to search, within a finite diffusion length, and diffuse to a final site with higher coordination number than at the original deposition site. In the case where there is no neighbor with higher coordination number, the adatom will remain at the deposition site. At the end of the diffusion process, the adatom becomes part of the substrate and the next adatom is deposited.

It is important to note that adatoms in the DT model search for final sites with higher coordination numbers compared to the deposition site. The final sites are not necessarily the local sites with maximum coordination numbers. In other words, in the DT model adatoms try to *increase*, but not necessarily *maximize*, the local coordination number. Also, deposited adatoms with more

than one nearest-neighbor bond do not move at all in the DT model.

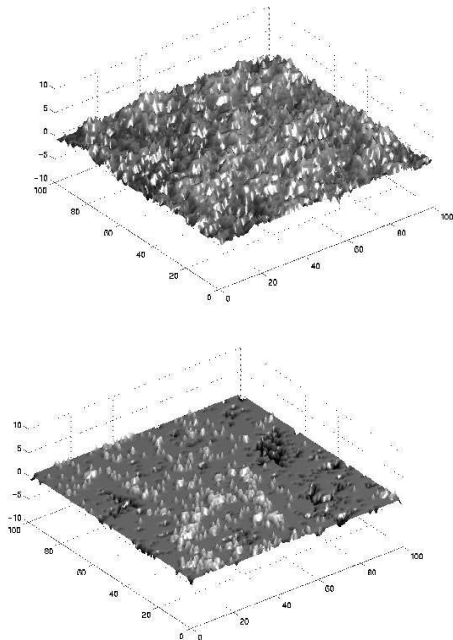


FIG. 3. Morphologies from F model with $n_r = 1$ (top) and $n_r = 5$ (bottom) from substrates of size $L = 100 \times 100$ after 10^6 ML.

3. Wolf-Villain model

The Wolf-Villain (WV) model [12] is very similar to the DT model in the sense that diffusion is controlled by the local coordination number. There are, however, two important distinctions between the two models. For one thing, in the WV model, an adatom with lateral nearest neighbors can still diffuse if it can find a final site with higher coordination number. The other difference is that, adatoms in the WV model try to *maximize* the coordination number, and not just to *increase* it as in the DT model (see Fig. 2). The two models have very similar behavior in one dimensional ($d=1+1$) simulations, and there have been substantial confusion regarding these two models in the literature. But in two dimensional ($d=2+1$) systems, after an initial crossover period, the two models behave very differently, as will be shown in this paper.

4. Kim - Das Sarma class of conserved growth models

A number of discrete growth models can be defined by applying the approach originally developed by Kim and Das Sarma [13] for obtaining precise discrete counterparts of continuum conserved growth equations. In this method, the surface current \mathbf{j} is expressed as the gradient of a scalar field K , which in turn is written as a

combination of h and its various differential forms, $\nabla^2 h$, $(\nabla h)^2$, ... etc., where certain combinations are ruled out by symmetry constraints:

$$\mathbf{j}(\mathbf{x}, t) = -\nabla K, \quad (4)$$

where

$$K = \nu_2 h - \lambda_4 \nabla^2 h + \lambda_{22} (\nabla h)^2 + \dots \quad (5)$$

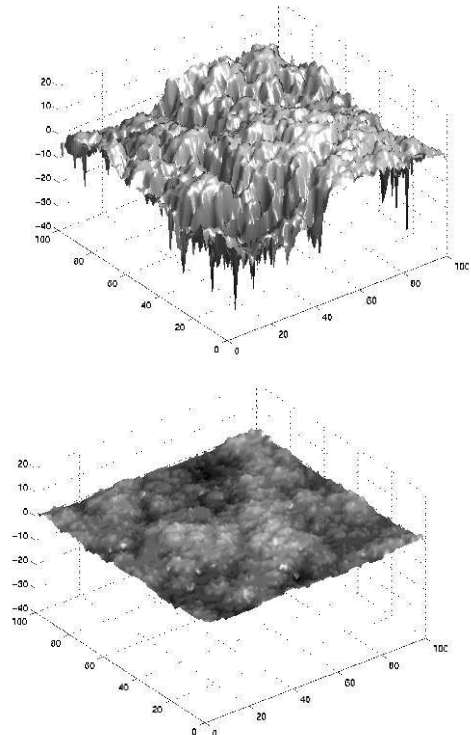


FIG. 4. Morphologies from DT model with $n_r = 1$ (top) and $n_r = 5$ (bottom) from substrates of size $L = 100 \times 100$ after 10^6 ML.

Using the above expression for K , the general conserved growth equation, Eq. (3), is obtained. Due to the conserved nature of growth, one concludes that the local particle transport happens in the direction of the largest variation of the scalar $-K$, i.e., in the direction where K has the largest decay. This allows for the definition of the following Kim-Das Sarma discrete atomistic rules: 1) a site i is chosen at random, 2) the scalar K is computed on the lattice at site i and for all its nearest neighbors, 3) then a particle is added to the site that has the smallest value of K ; if site i is among the sites with the smallest K , then the particle is deposited at site i , otherwise one picks a final site with equal probability among those sites that have the common smallest K .

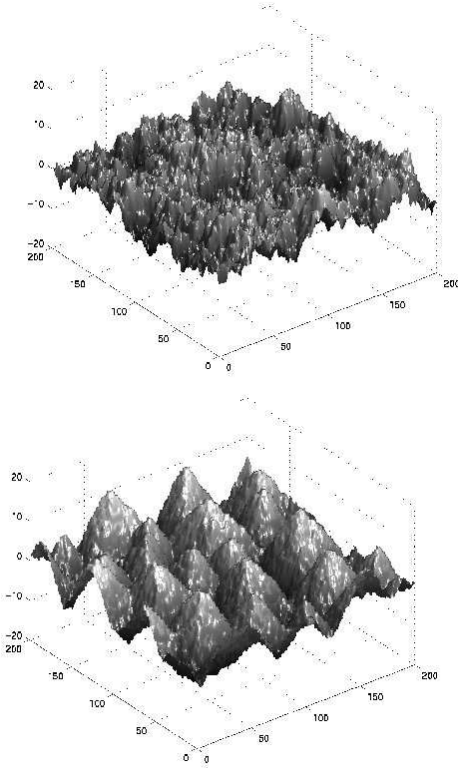


FIG. 5. Morphologies from WV model with $n_r = 1$ (top) and $n_r = 5$ (bottom) from substrates of size $L = 500 \times 500$ after 10^4 ML.

For example, the F model (where adatoms relax to the sites with local height minima) is described by the linear second order growth equation, with $K \sim h$ in Eq. (5). Thus the well-known F model obeying the linear EW equation is the simplest example of the Kim-Das Sarma class of discrete growth models. A well-known member of the Kim - Das Sarma class is the *Larger Curvature model* (LC) [13,14] where $K \sim -\nabla^2 h$ (which generates the linear fourth order growth equation). Adatoms in this model diffuse to sites with minimum $-\nabla^2 h$, i.e. with maximum curvature, hence the name of the model.

In this paper we also study the nonlinear fourth order equation [8,15] where:

$$K = -\lambda_4 \nabla^2 h + \lambda_{22} (\nabla h)^2 \quad (6)$$

with λ_{22} being a small constant controlling the instability in the equation. Recently, a nonlinear fourth order equation with controlled higher order nonlinearities [16,17] has been proposed as a continuum description for the DT model. The scalar K in this equation is

$$K = -\lambda_4 \nabla^2 h + \frac{\lambda_{22}}{C} [1 - e^{-C|\nabla h|^2}]. \quad (7)$$

The last variant we analyze is the the linear sixth order continuum growth equation, with $K \sim -\nabla^4 h$.

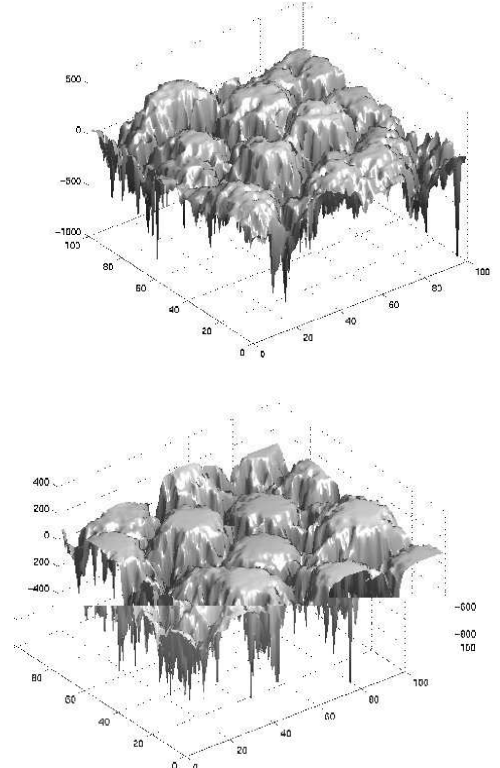


FIG. 6. Morphologies from DT model in the presence of an ES barrier with $n_r = 1$ (top) and $n_r = 5$ (bottom) from substrates of size $L = 100 \times 100$ after 10^6 ML.

B. The noise reduction technique

In this section we briefly discuss a well-known theoretical method used to reduce stochastic noise in the stochastic growth simulations of surface morphologies, in particular its short wavelength component. The short wavelength noise component generates an intrinsic width (w_i) in the surface roughness giving rise to strong nontrivial corrections to scaling [18], and typically has different scaling properties than the long wavelength quantities, such as the dynamical width ($w \sim t^\beta$) and the correlation length parallel to the surface ($\xi \sim t^{1/z}$). Reducing the intrinsic width through the noise reduction technique, the scaling behavior improves dramatically, and the asymptotic critical properties emerge in the simulations [18–20]. In the simplest growth models of MBE, two main competing kinetic processes are kept and simulated: (1) deposition from an atomic beam, and (2) surface diffusion of the freshly landed atoms until they incorporate into the surface according to some diffusion rules. The shot noise in the beam is simulated in (1) by randomly selecting the landing site, and the surface diffusion performed by the freshly landed atoms is simulated in (2) essentially by a random walk of l steps biased by the local coordination (filled and unfilled sites) landscape of the surface.

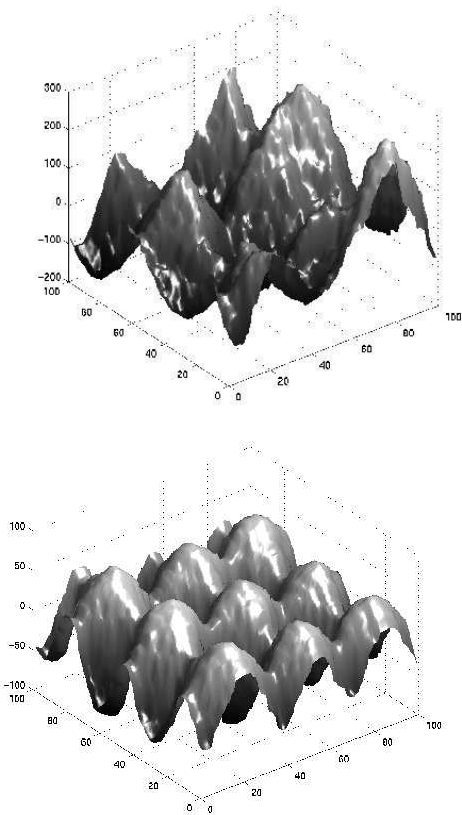


FIG. 7. Morphologies from WV model in the presence of an ES barrier with $n_r = 1$ (top) and $n_r = 5$ (bottom) from substrates of size $L = 100 \times 100$ after 10^6 ML.

The noise reduction method, originally introduced [19,20] to study the Eden model, proceeds as follows: a site is chosen randomly (with uniform probability L^{-d}), then the l -step random walk (“diffusion”) is performed according to the local diffusion rules of the model. Assume that the site where the atom would be incorporated is site i . Instead of actually depositing the atom at site i , first a counter c_i associated with site i is increased. The deposition attempt becomes a “true” deposition process only if the counter at the attempt site reaches a predetermined threshold value n_r . After a true deposition the counter is reset to zero, and the process is repeated. The integer n_r is the *noise reduction factor* and it quantifies the level of noise suppression, larger values meaning a stronger suppression. Obviously $n_r = 1$ simply means that there is no noise reduction. The noise reduction technique has been successfully used in limited mobility MBE growth models [18,21]. The effects of noise reduction can also be understood as a coarsening process, as shown in Ref. [7]: noise reduction performs an effective coarsening of the shot noise within regions of linear size ℓ , which is defined as the linear distance within which no nucleation of new islands can form on the terraces.

An important observation is that when the noise reduction technique (NRT) is used, the ‘material param-

eters’ such as the noise strength, diffusion constant, step stiffness, etc. in general become dependent on the level of noise reduction [7], which is quantified by the noise reduction parameter n_r .

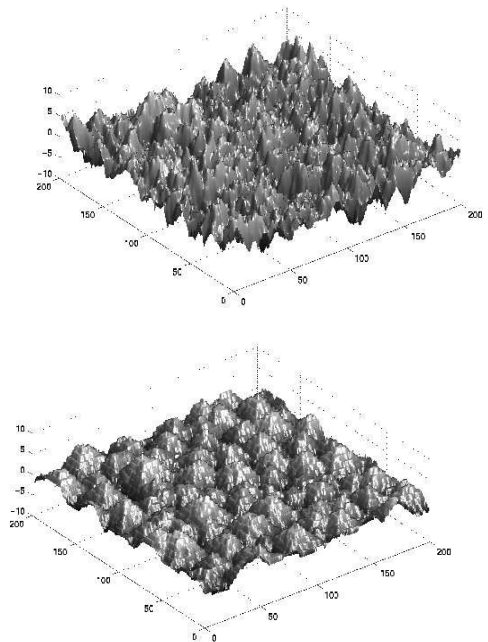


FIG. 8. Morphologies from LC model with $n_r = 1$ (top) and $n_r = 8$ (bottom) from substrates of size $L = 200 \times 200$ after 10^3 ML.

Brendel, Kallabis and Wolf have recently identified [7] the dependence of the material parameters on the level of noise reduction for kinetic roughening described on coarse-grained scale by the KPZ equation, $\frac{\partial h}{\partial t} = \nu \nabla^2 h + \lambda (\nabla h)^2 + F\Omega + \eta$ in the context of layer-by-layer growth. In this case it turns out that the parameters ν and λ assume power law behavior: $\nu \sim (n_r)^{e_\nu}$ and $\lambda \sim (n_r)^{e_\lambda}$, where the exponents are not universal and may depend on the details of the way in which the model is simulated. A simple argument by Kertész and Wolf [19] shows that the noise strength D is weakened by NRT according to:

$$D(n_r) \propto 1/n_r. \quad (8)$$

Two of the current authors have earlier studied [18] the effect of noise reduction in the growth simulations of limited mobility DT, WV, and F models, finding that NRT is extremely effective in suppressing crossover and correction to scaling problems in these growth models, leading effectively to the asymptotic critical exponents rather compellingly. An important feature of the current article is to obtain simulated 2+1-dimensional growth morphologies of the various growth models under NRT. We find that NRT is extremely effective in suppressing noise and giving rise to the epitaxial mounded morphologies in models where SED mechanism is operational.

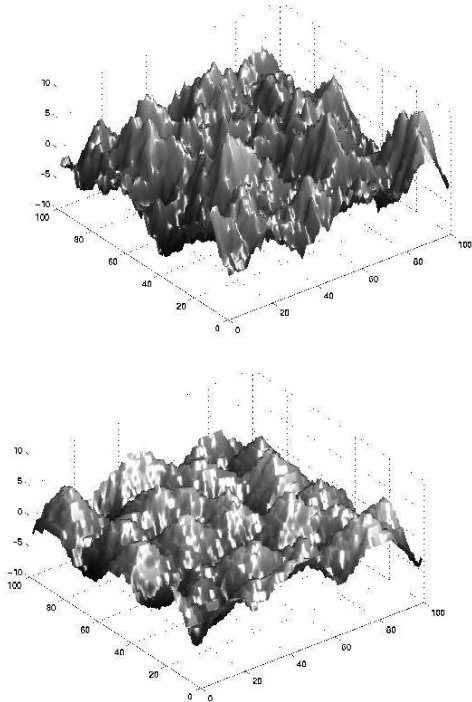


FIG. 9. Morphologies from nonlinear fourth order model with $n_r = 1$ (top) and $n_r = 5$ (bottom) from substrates of size $L = 100 \times 100$ after 10^3 ML. The coefficient of the nonlinear term is $\lambda_{22} = 0.5$.

Often (almost always) the limited mobility models of interest in our paper are far too noisy (because of the extreme limited role of diffusion in the models) to exhibit epitaxial mounding without effective noise reduction, at least in treatable simulation times.

C. Growth morphologies

In this section, we show simulated dynamical growth morphologies of the discrete SOS models described earlier, with and without NRT.

The first model is the F model which is known to be described exactly by the linear second order growth equation and belong to the well known EW universality class. As shown in Fig. 3, F morphology with $n_r = 1$ (without NRT) is already quite smooth. However, when noise is suppressed with $n_r = 5$, the layer-by-layer growth process persists as long as 10^6 monolayers, which is our longest simulation time for the system. With layer-by-layer growth, the interface is extremely smooth and flat and this agrees with the EW universality definition where the growth (β) and the roughness (α) exponents in 2+1 dimensions is zero corresponding to smooth growth.

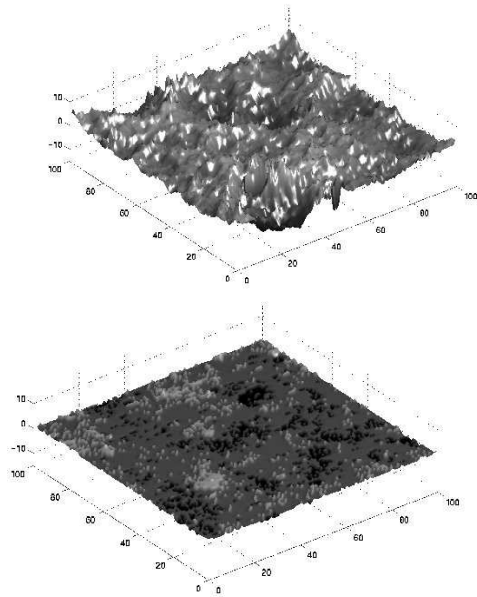


FIG. 10. Morphologies from nonlinear fourth order model with an infinite series of higher order nonlinear terms with $n_r = 1$ (top) and $n_r = 5$ (bottom) from substrates of size $L = 100 \times 100$ after 10^3 ML. The coefficients of the nonlinear term are $\lambda_{22} = 5.0$ and $C = 0.085$.

The DT model, as shown in Fig. 4, shows kinetically rough interface in the $n_r = 1$ simulation. But with $n_r = 5$, the morphology becomes considerably smoother, without any specific mounding pattern. Similar to the DT model, the WV model (Fig. 5) with $n_r = 1$ shows rough morphology without any special mounding features. But when we suppress the noise, using $n_r > 1$, the WV morphology changes drastically and patterned mound formations can clearly be seen. This mound formation in the WV model is intriguing because there is no ES barrier involved in the simulation. As it turns out, the WV diffusion rule has an intrinsic mechanism to create a local uphill particle current which is strong under NRT, and hence a pyramid-like mounded morphology formed. This topic is discussed in the next section.

We have actually carried out both DT and WV model growth simulations [21] in the presence of an ES barrier also. For the sake of comparison with the epitaxial mounding in the WV model without any ES barrier (but with NRT), as shown in Fig. 5, we present in Figs. 6 and 7 the observed mounded morphologies in the DT and WV models in the presence of an ES barrier (both with and without NRT). One can clearly see that the ES barrier induced mounding instability in Figs. 6 and 7 is qualitatively different from the epitaxial mounding in Fig. 5. While the ES barrier induced DT/WV mounding has flat tops, the intrinsic WV mounding of Fig. 5 is of pyramid shape.

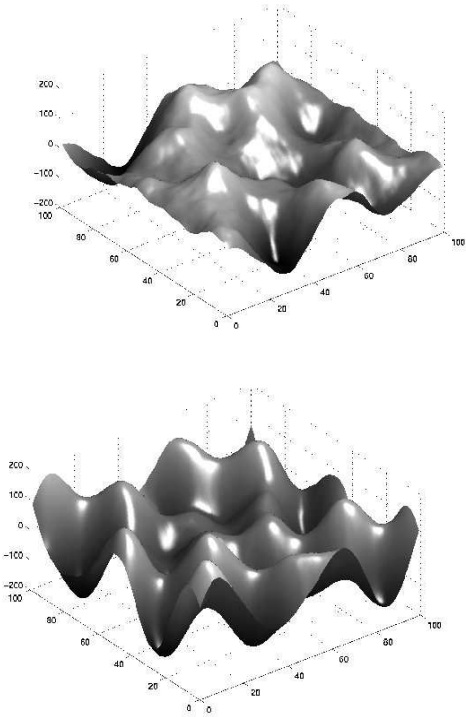


FIG. 11. Morphologies from linear sixth order model with $n_r = 1$ (top) and $n_r = 5$ (bottom) from substrates of size $L = 100 \times 100$ after 10^6 ML.

The linear fourth order model (the LC model) also creates mounds without ES barrier in a way similar to the WV model. This is shown in Fig. 8 (and also Fig. 1).

Although the epitaxial mounding in Figs. 5 and 8 look similar, the mounded morphologies in LC and WV models are not identical, however, as the LC is a linear model and hence the morphology exhibits up-down symmetry, while the WV morphology does not look the same when it is turned upside down, and therefore does not possess the up-down symmetry. This lack of up-down symmetry in the WV model arises from the presence of the nonlinear $\nabla^2(\nabla h)^2$ term in its dynamics. When we add a small instability into the LC equation, by adding the nonlinear fourth order term with a small coefficient, the interface (shown in Fig. 9) is somewhat mounded even for $n_r = 1$ simulation. But the surface in this $n_r = 1$ model is so rough that a specific mound pattern cannot be discerned. When we reduce the noise, using $n_r = 5$, clear mound formation (without up-down symmetry) can be seen in the morphology as one would expect.

In Fig. 10 we present our simulation results for the full nonlinear equation (Eq. (7) with $C = 0.085$) with an infinite number of nonlinear terms. The rationale for studying this particular continuum equation with an infinite number of nonlinear terms of the $\nabla^{2n}(\nabla h)^{2n}$ form is the fact that recently it has been established [16,17] that such as infinite order nonlinear dynamical equation is the

most likely continuum description (at least in $d=1+1$ dimensions, where this issue has so far been studied intensively) of the discrete DT model.

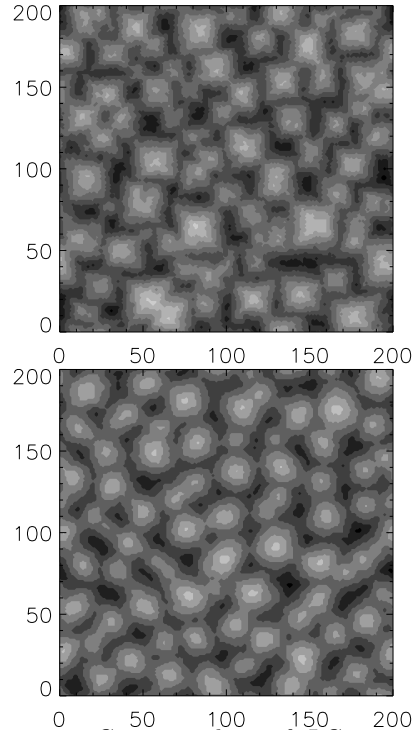


FIG. 12. Contour plots of LC morphologies from $L = 200 \times 200$ at 10^3 ML with $n_r = 8$. Lighter (darker) shade represents higher (lower) points. Plot (a) corresponds to the “higher priority” version while plot (b) is from the “equal priority” version. Here $l = 1$.

Since the DT model does not seem to exhibit (see Fig. 4) any epitaxial mounding instability in our simulations, it is of considerable interest to see how the infinite order nonlinear continuum equation behaves. It is, therefore, gratifying to see, as shown in Fig. 10, that the growth morphology in the infinite order nonlinear equation does not exhibit any discernible mounding patterns — the morphologies depicted in Fig. 10 look vaguely similar to the kinetically rough growth of the DT model shown in Fig. 4. It is, however, remarkable that the fourth order continuum equation (either the linear LC model as in Figs. 1 and 8 or the nonlinear model with a small nonlinearity as in Fig. 9) manifests striking mound formation, but the infinite order nonlinear equation does *not* manifest any epitaxial mounding. We do not have a precise mathematical understanding of this dichotomy other than pointing out that the presence of an infinite series of nonlinear terms clearly overwhelm the SED instability arising from the $\nabla^4 h$ surface diffusion term. The precise understanding of the combined effects of noise reduction and growth nonlinearities is not available at the present time. Finally, in Fig. 11 we present the surface morphologies associated with the linear sixth order growth

equation. The mounding pattern can be barely seen in the $n_r = 1$ simulation. But the spectacular mound formation can be seen clearly when we reduce the noise ($n_r = 5$).

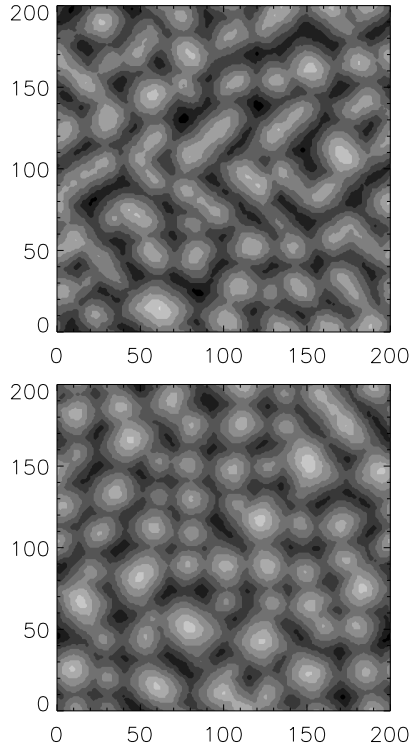


FIG. 13. Contour plots of LC morphologies from $L = 200 \times 200$ at 10^3 ML with $n_r = 8$. Lighter (darker) shade represents higher (lower) points. Plot (a) corresponds to the “higher priority” version while plot (b) is from the “equal priority” version. Here $l = 2$

These simulated morphologies are very sensitive to the local atomistic diffusion rules, as can be seen when we make some minor modifications to the LC rule. The first thing we modify is to make the adatoms more “energetic”. In the original LC model, an adatom searches for a site with the largest curvature, and if the original random deposition site is one of the sites with the largest curvature then the adatom remains at the deposition site. So in the original version of the model, an adatom will not move if it is already at one of the preferred sites. We call this original model the “higher priority” version of the LC model, as the deposition sites have *higher priority* than the neighboring sites. In the modified version, called “equal priority” version, the adatom chooses its final site among all the sites with largest curvature with equal probability. So even if the original deposition site is one of the largest curvature sites, the adatom may still end up being incorporated at a neighboring site if that neighbor also has the same curvature as the deposition site. The second modification we make is simply to increase the diffusion length l from nearest-neighbor-only

diffusion ($l = 1$) to $l > 1$ where diffusion rules now extend to $l(> 1)$ sites.

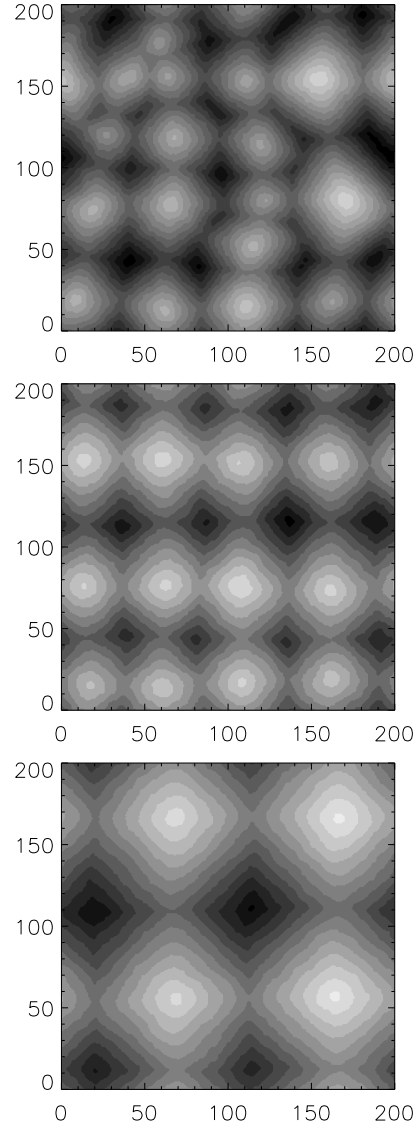


FIG. 14. Contour plots of “equal priority” LC model with $l = 2$ and $n_r = 8$ at (a) 10^4 ML, (b) 10^5 ML and (c) 10^6 ML.

It is known [11] that increasing diffusion length does not change the asymptotic universality class of limited mobility growth models as long as the substrate size is large enough so that finite size effects remain negligible. But increasing diffusion length can most certainly change the early-time morphology of the system by strongly affecting finite size effects.

Both versions of LC model show mounded morphologies, as can be seen in Fig. 12. But it seems that the “equal priority” version, the one with more energetic adatoms, has mounds with the bases lined in the 110 direction. In the “higher priority” version the mounds are more stable when the bases are in 100 direction. Increas-

ing diffusion length in the simulations encourages faster coarsening process (Fig. 13), as should be expected, and individual mounds in the $l = 2$ simulations “link” to each others more than in the $l = 1$ simulations. To further investigate the mound coarsening process, we study the “equal priority” LC model with $l = 2$ in long time limit and find that the mounds rearrange themselves into a regular pattern as shown in Fig. 14. This regular rearrangement of the mound morphology, caused by longer diffusion lengths as well as the different symmetry properties (110 versus 100) of the equal priority and higher priority LC models, show the extreme sensitivity of the epitaxial mound morphology to the details of the diffusion process controlling growth — in general, we find the SED instability in all our simple models to be quite complex in the sense of the mound patterns (and even whether mounds exist or not as in WV and DT models) seem to be very sensitive to the details of the surface diffusion rules.

III. KINETIC-TOPOLOGICAL “INSTABILITY”: STEP-EDGE DIFFUSION

A. A continuum description

It has been recently recognized [4] that step-edge diffusion generates a local *uphill* surface diffusion current during the deposition process, leading to a morphological “instability”, i.e. the starting substrate is no longer stable after growth. This instability is purely of topologic-kinetic nature, and it is *not* generated by an energetic instability such as the Ehrlich-Schwoebel instability. It is rather a consequence of the fact that surface diffusion currents (in two or higher dimensions) are vectorial quantities, and while some of their components have a smoothening and stabilizing effect in a certain subspace, in other directions they may act as instabilities, as is shown schematically in Fig. 15. This figure is a top view of a two dimensional substrate on which there are two vicinal surfaces. Due to diffusion, the adatoms on the flat terraces may reach the edge of the terrace, however they are assumed to feel no energetic barriers at the step edges. After reaching the edge of the step the adatoms will tend to remain attached to it since it is an energetically more favorable position (with at least one more extra bond when compared to the position on the terrace). The atoms on the step edge may relocate through *line-diffusion* along the edge to energetically even more favorable places (kink sites), thus reducing the differences in the local chemical potential. (For simplicity we assume no desorption from the growth front.) For example, if there is a protuberance on (or a dent in) the step as shown in Fig. 15 (a), the step-edge atoms will preferentially diffuse towards the base of the hump (or towards filling up the dent), creating a net current towards the

region of larger height, i.e. *uphill* as shown by the thick white arrow in Fig. 15 (a).

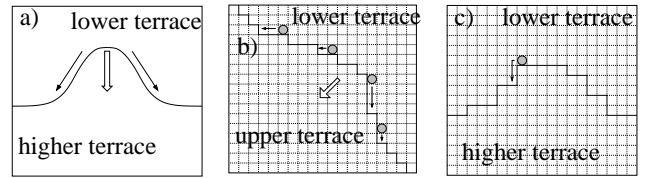


FIG. 15. Schematic illustration of the instability caused by the line tension in the step-edge. View from above, the thick line is the boundary between two terraces whose difference in elevation is one monoatomic layer. a) shows a continuum picture while b) and c) represent the same on a lattice for different step-boundary orientations.

Note that although this current stabilizes the step-edge, it *destabilizes* the $2 + 1$ dimensional surface $h(x, y)$ at long wavelengths, creating mounds on the substrate induced by the uphill current. The local current density \mathbf{J}_1 along the edge of the chemical potential μ , i.e., one can write $\mathbf{J}_1 = -\nu \nabla_\epsilon \mu$, where ν is the mobility of the atoms along the step edge [22]. Assuming local thermodynamic equilibrium, the chemical potential may be expressed as a functional of a free energy which in turn is written as that of an elastic line of line-tension σ . The result is that μ is proportional to the local curvature κ of the line, $\mu = -\sigma \kappa$ [22]. κ is the local curvature on the line $h(x, y) = \text{const}$, and thus it can be expressed in terms of the local derivatives of h :

$$\mathbf{J}_1 = -\sigma \nu \nabla \left(|\nabla h|^{-3} \begin{vmatrix} h_{xx} & h_{xy} & h_x \\ h_{yx} & h_{yy} & h_y \\ h_x & h_y & 0 \end{vmatrix} \right) \quad (9)$$

Next, we calculate the uphill current due to the current density (in Eq. (9)) created by an arbitrary shaped hump created at the edge of a single straight step, and then specialize the expression for a simple, cosine shaped hump. We assume that one can choose an (x, y) coordinate system such that the equation for the step-profile $h(x, y) = \text{const}$ in this system is simply expressed by a single valued function: $y = y(x)$, see Fig. 16. In this simple setup the edge is parametrized by x , and thus the step-edge current in Eq. (9) becomes:

$$\mathbf{J}_1 = \nu \sigma \frac{y^{(3)} [1 + (y')^2] - 3y'(y'')^2}{[1 + (y')^2]^{7/2}} (\mathbf{e}_x + y' \mathbf{e}_y) \quad (10)$$

where $y^{(3)}$, y'' and y' are the third, second and first order derivatives of the profile, and \mathbf{e}_x and \mathbf{e}_y are the unit vectors along the x and y axes, respectively. The total mass transported per unit time by curvature gradients between points A and B on the step-edge is defined as

the line-integral of the edge current density:

$$\mathbf{I}_{AB} = \int_A^B ds \mathbf{J}_1 \quad (11)$$

where ds is the integration element along the curve of the step-edge. In the following we illustrate that this current points toward the base of the higher step.

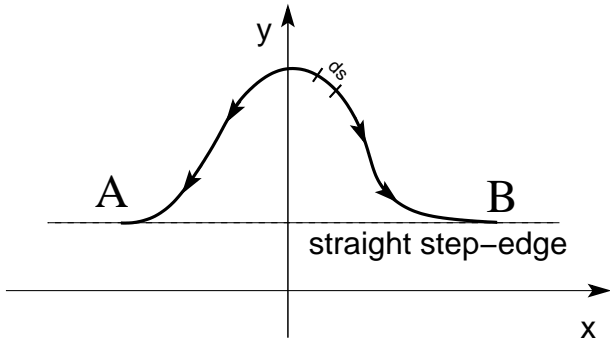


FIG. 16. A straight step-edge with a hump. The step-edge current density generated by the local curvature gradient along the hump creates a net uphill current.

Let us choose a step-profile given by $y(x) = a \cos(bx)$ between the points $x_A = -\pi/b$ and $x_B = \pi/b$. After performing the integrals in Eq. (11), one obtains:

$$\mathbf{I}_{AB} = -\frac{4\nu\sigma b}{15} \left[\frac{1 + 11z + 6z^2}{(1+z)^2} \mathbf{E}(i\sqrt{z}) - \frac{1 + 3z}{1+z} \mathbf{K}(i\sqrt{z}) \right] \mathbf{e}_y \quad (12)$$

where $z = a^2b^2$ is a dimensionless number, and $\mathbf{K}(k)$ and $\mathbf{E}(k)$ are complete elliptic integrals of first and second kinds respectively. Since $1 + 11z + 6z^2 > 1 + 4z + 3z^2$, and $\mathbf{E}(i\sqrt{z}) > \mathbf{K}(i\sqrt{z})$, for all $z > 0$, the mass-current has a negative y component (the x component is zero because of symmetry), i.e., it points towards the base of the higher step, uphill. In the limit of small humps, $z \ll 1$ (small slopes approximation), $\mathbf{K}(i\sqrt{z}) \simeq \frac{\pi}{4}(1 - \frac{z}{4})$, $\mathbf{E}(i\sqrt{z}) \simeq \frac{\pi}{4}(1 + \frac{z}{4})$, so the current becomes proportional to the square of the hump's height, $I_{AB} \sim -\pi\nu\sigma b^3 a^2$ and for peaked humps ($z \gg 1$), $\mathbf{K}(i\sqrt{z}) \simeq \ln(4\sqrt{z})/\sqrt{z}$, $\mathbf{E}(i\sqrt{z}) \simeq \sqrt{z}$ the current depends linearly on the height of the hump, $I_{AB} \sim \frac{8}{5}\sigma\nu b^2 a$. The same analysis can be repeated when there is a dent in the step profile, with similar conclusions. Certainly, the currents expressed above are instantaneous local currents. If one is interested in the evolution of the step profile, one can employ simple geometrical considerations (see [22,23]) to write:

$$\frac{\partial y}{\partial t} = v_n \sqrt{1 + (y')^2} \quad (13)$$

where $y = y(x, t)$, v_n is the normal step-edge velocity and the prime denotes derivative with respect to x .

Assuming that the mass transport is solely due to the step-edge current, one has $v_n ds = -(\partial J_l / \partial x) dx$, with $ds = dx \sqrt{1 + (y')^2}$. Thus Eq. (13) takes the form:

$$\frac{\partial y}{\partial t} = -\frac{\partial J_l}{\partial x} = -\nu\sigma \left(\frac{y^{(4)}}{[1 + (y')^2]^2} - \frac{10y'y''y^{(3)}}{[1 + (y')^2]^3} - \frac{3[1 - 5(y')^2](y'')^3}{[1 + (y')^2]^4} \right). \quad (14)$$

In the limit of small slopes, $y' \ll 1$, $y'' \ll 1$, $y^{(3)} \ll 1$, $y^{(4)} \ll 1$, and so from Eq. (14) it follows that: $\partial y / \partial t = -\nu\sigma y^{(4)}$, after keeping the leading term only. This is the well known Mullins equation for the dynamic relaxation of a step-edge, related to the fourth order linear growth equation, Eq. (6) with $\lambda_{22} = 0$, followed by the LC model in our growth simulations.

The continuum description presented here compellingly demonstrates the possibility of a destabilizing uphill current arising entirely from step edge diffusion — an SED instability without any ES barriers, as discussed in Refs. [4,5] recently.

B. A discrete description

In reality the deposition process (and our simulation of limited mobility models) takes place on the discrete and atomistic crystalline lattice, which introduces an orientation dependence of the line tension σ . One would naturally expect that the high-symmetry, in-plane crystalline directions will have the largest σ , these being the most stable. However, there is a hierarchy even among these high-symmetry orientations, as is illustrated in Figs. 15 (b) and 15 (c). Fig. 15 (b) shows a step-edge aligned along a diagonal of the square lattice and in Fig. 15 (c) the step-edge is oriented along one of the main axes of the lattice. While the step is stable along the diagonal, it is not as stable along the main axis, since in this latter case (of Fig. 15 (c)) in order for an atom to reach a higher coordination site along the line, it has to detach itself from the step-edge (to become an adatom) first, which is energetically less favorable.

Let us now analyze in more detail the effects of SED in the case of the two most important MBE-motivated limited mobility models, WV and DT models. The diffusion rules for the mobile atoms for these two models are only slightly different: in the case of WV model particles seek to maximize their coordination while in the DT model they only seek to increase it. Nevertheless the two models present completely different behaviors. As we have seen in Subsection II.C, the NRT version of WV model produces mounded structures, however this does not happen for the DT model. In the following we explain this unexpected difference between WV and DT models based on local SED currents. Given the rather “minor” differences between DT and WV rules (and their

almost identical growth morphologies in 1+1 dimensions) it is remarkable how different their 2+1 dimensional NRT growth morphologies are (WV has spectacular mounded morphology as seen in Fig. 5 and DT has essentially statistically scale invariant kinetically rough growth as in Fig. 4).

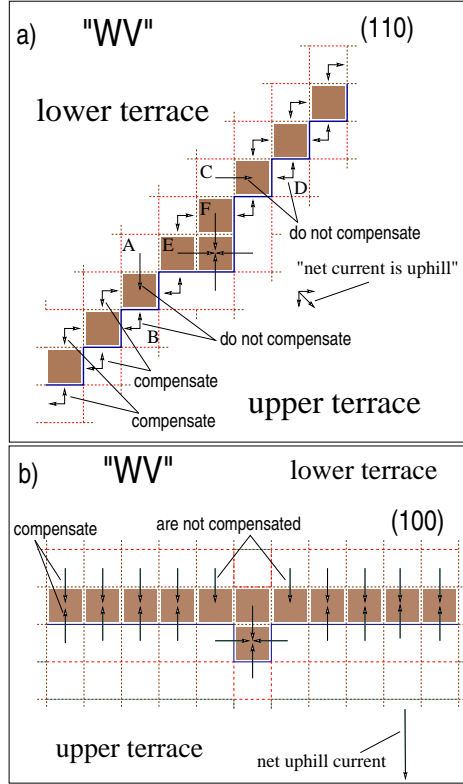


FIG. 17. Local currents along step-edges of orientations (110) and (100) for the WV rules.

Providing an understanding of this difference (between DT and WV morphologies) in terms of the SED instability (WV has it and DT does not) is one of the important accomplishments of our work.

Figs. 17 and 18 show two high-symmetry oriented steps, (110) and (100) respectively, with a small dent in it. The local particle current shown by arrows are calculated using the rules of WV and DT models. One can immediately conclude that in the case of these configurations, the net current is $j_{(111)}^{WV} = \sqrt{2}/2$ and $j_{(100)}^{WV} = 2$ both directed *uphill*, $j_{(111)}^{DT} = -\sqrt{2}/2$ directed *downhill* and $j_{(100)}^{DT} = 1/3$ directed uphill. (The current is considered to be 1 across the boundary between nearest neighbor sites X and X', if a particle once at position X will go in one step with probability 1 to position X'. In case of ties, the probability fraction corresponding to the rules is taken).

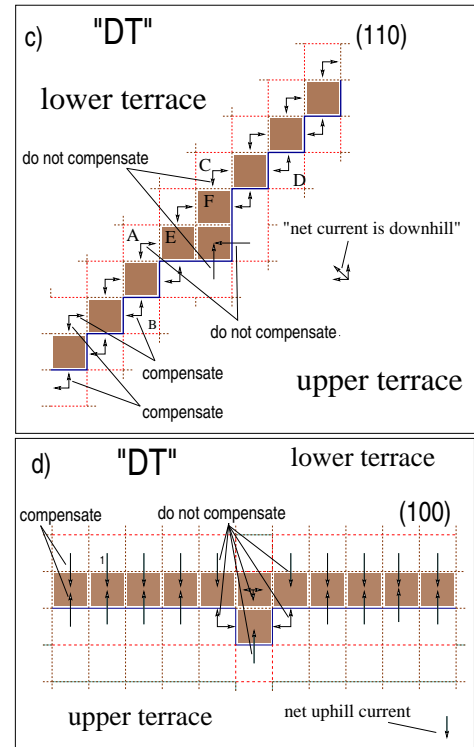


FIG. 18. Local currents along step-edges of orientations (110) and (100) for the DT rules.

As seen from the configurations above, there is a clear net uphill local current in the case of WV model in both cases of high-symmetry orientations. According to the theory of SED, one should see a mounded morphology. Nevertheless, when we look at the morphology of Fig. 5 (a), one only sees a rough surface not obviously a mounded landscape in the $n_r = 1$ WV growth. The reason for this discrepancy lies at the heart of the SED instability and the conditions (and constraints) for its observability: having destabilizing step-edge diffusion currents is *not sufficient* for the creation of mounds. There is another very important necessary ingredient (which was not analyzed in Refs. [4,5]) that is needed for the formation of quasi-regular mounded growth patterns in addition to the destabilizing SED currents: *suppression of deposition and nucleation noise*. In order to have a consistent uphill current build-up (to create mounds), we need a sustained stability of the step-edge, in other words, if we look at the step-edge as a 1+1 dimensional 'surface' in the $x-y$ plane (the upper terrace being the 'substrate') we need to have more or less a solid-on-solid type of step-edge, with perhaps some small overhangs eventually, but no large or frequent ones. The only effect which can disrupt a stable step-edge is the *nucleation of new islands* on the terraces near the edge. Let us imagine that we start with a straight step, aligned along the most stable direction. If island nucleation takes place easily, then the islands that nucleate close to the stable edge will quickly grow into the step, disrupting the step's contour and identity. If the re-

laxation time of the disrupted contour is larger than the nucleation time, small newly grown islands will disrupt the step even further until it ceases to exist. In this case the SED instability *will not* manifest in the mound formation because the necessary condition for mound formation is not satisfied globally although there may be local uphill current. Thus, noise may prevent the SED instability from manifesting a global mounded instability.

The importance of noise suppression for the SED instability is strikingly apparent from comparing Figs. 5 (a) and 5 (b) for the WV model. The NRT version has mounded morphology and the $n_r = 1$ version does not. However for the DT model, one finds no such regular mounded structures even when noise and nucleation is strongly suppressed (Fig. 4). The reason for this difference is that in the DT model the SED current is essentially downhill (and thus is stabilizing). Depending on the edge configuration (for example the (100) edge in Fig. 18) one may find a *small* uphill current in the DT model, however it is statistically not significant to destabilize the whole surface. There will be a weak mounding tendency at early times, when the $\nabla^4 h$ diffusion term is relevant and when the height-height correlation function shows some oscillations (see [6]), indicating the presence of this term, but then it will be quickly taken over by the stabilizing downhill current and nucleation events. Thus, the DT model, at best, will exhibit some weak and irregular epitaxial mounding [6], but *not* a regular patterned mounded morphology.

Another important point is that mounding due to the SED instability *does not require any growth nonlinearity to be present*. This is obvious from the fact that the LC model, which is strictly linear by construction, shows spectacular epitaxial mounding induced by the SED instability. In the following subsection we analyze in more details the effects of noise reduction on the SED instability.

C. Noise reduction method: a numerical way to control the step edge diffusion instability

As emphasized in the previous subsection, a necessary ingredient for creating mounds by SED is the suppression of noise. In the following we restrict our analysis to discrete limited mobility models, and frequently use for comparison WV and DT models. Unfortunately, rigorous analytical calculations are practically impossible for discrete and nonlinear dynamical growth models of DT and WV types. However, we make an attempt by introducing the proper quantities to pinpoint the effects of noise reduction on these two models and actually show the major difference between the two models in one and two substrate dimensions in the context of SED instability. First, we introduce the notion of *conditional occupation rates*. The conditional occupation rate f_i associated with site

i in a particular height-configuration is the *net gain* of transition rates coming from the contribution of all the neighbors within a distance of l sites on the surface and from the growth direction (from the deposition beam).

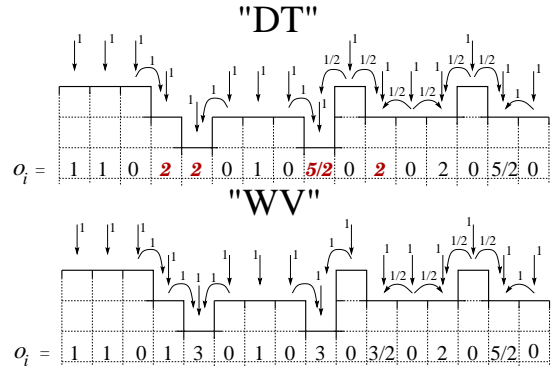


FIG. 19. Conditional occupation probabilities for two particular configurations in 1 + 1 dimensions for DT and WV models. The f_i -s that differ for the DT from WV are set in bold italics. Here $l = 1$.

The f_i -s can easily be calculated once the diffusion rules are known. If $\mathcal{W}_{i \rightarrow i'}$ is the transition rate for an atom landed on site i to be incorporated at site i' (which is a nearest neighbor when $l = 1$), then:

$$f_i = 1 + \sum_{i'}^{\{i\}_l} (\mathcal{W}_{i' \rightarrow i} - \mathcal{W}_{i \rightarrow i'}) \quad (15)$$

where the unity in front of the sum represents the contribution from the beam and $\{i\}_l$ means summing the contributions over all the neighbors of site i within a distance l . The f_i -s are obviously conditioned to the event that there is an atom landed on site i or on the neighbors i' . It is important to emphasize that these quantities in Eq. (15) are introduced for the no-desorption case only: once an atom is incorporated in the surface it stays that way. If one wishes to add desorption to the model, then the evaporation rates have to be included in Eq. (15) as well (the rates in Eq. (15) are all diffusion rates).

Let us now illustrate in light of the two models WV and DT, the conditional occupation rates, in 1+1 and 2+1 dimensions. Figs. 19 and 20 show the f_i -s for particular configurations for one and two dimensional substrates respectively. The fractional transition rates mean that the motion of the atom is probabilistic: it will choose with equal probability among the available *identical* states. This is in fact the source of the diffusion noise η_c , arising from the stochastic atomistic hopping process, which should be added to the right hand side of Eq. (1), however, it is an irrelevant contribution in the long wavelength scaling in the renormalization group sense. The conditional occupation rates f_i are small rational num-

bers from the interval:

$$f_i \in [0, Z_l^{(d)} + 1] \quad (16)$$

where Z_l is the maximum l th order coordination number on the d -dimensional substrate.

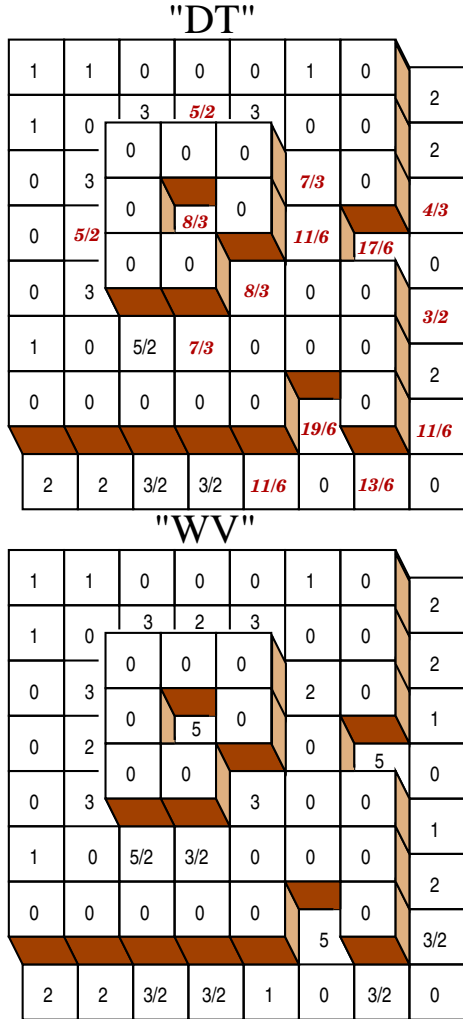


FIG. 20. Conditional occupation probabilities for two particular configurations in $2 + 1$ dimensions for DT and WV models. The f_i -s that differ for the DT from WV are set in bold italics. Here $l = 1$.

For example, on a cubic lattice, $Z_1^{(d)} = 2d$. For a fixed set of deposition and diffusion rules the number of possible occupation rates is fixed, and for low l -values it is only a few. This number is determined by how many different values can be obtained from all the possible relative height combinations of all sites within a d -dimensional ball of radius $2l + 1$ (the gain coming from the neighbor at l -away may depend on the configuration of radius l around that neighbor). If $l = 1$ then in $1 + 1$ dimensions this means that a chain of maximum 7 sites has to be considered and in $2 + 1$ dimensions it is a square domain of maximum 25 sites to exhaust all the possibilities (the

domain in this latter case is given by all (i, j) sites that obey $|i| + |j| \leq 3$). For example, the one dimensional WV model will have conditional occupation rates from the set $\{0, 1/2, 1, 3/2, 2, 5/2, 3\}$. For the one dimensional DT, the set is a bit restricted: $\{0, 1, 3/2, 2, 5/2, 3\}$, it does not allow for $f = 1/2$.

Fig. 21 shows the plot for the occurrence probabilities $p(f)$ versus the conditional occupation rates for both the WV and DT models ($n_r = 1$). The occurrence probability of rate f in one dimension is calculated as follows: take all the possible height configurations that are distinguished by the deposition and diffusion rules, (e.g. WV and DT) of the $2(2l + 1) + 1$ sites, monitor the f that belongs to the middle site and then measure the rate of occurrence of each value for f .

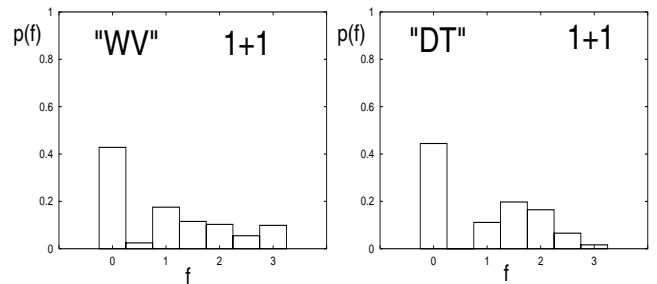


FIG. 21. Conditional occupation rates and their occurrence probability $p(f)$ for the WV and DT models. Here $l = 1$.

It is important to count these occurrences relative to the distinguishable number of configurations. Both WV and DT models have their rules for the motion of the landed atom formulated in terms of *coordination numbers*. In the WV model, the landed atom will move to the site with the maximum coordination whereas in DT the atom will move to increase its coordination. Thus only those configurations will be distinguished by the rules that have different coordination numbers in at least one of the sites. A given set of coordination numbers thus determines a class of configurations. For example in $1 + 1$ dimensions both the WV and DT models on 7 sites will distinguish a total of $3^6 = 729$ classes, since the deposition and diffusion rules for these two models do not involve actual height differences, just the fact that a site is at higher, the same, or lower level than its neighbors. In $2 + 1$ dimensions the exact enumeration of these classes is highly non-trivial, and it constitutes the subject of a future publication.

One can note the following property of conditional occupation rates: in every domain of sites on the substrate that has a zero inflow and zero outflow current across its boundaries ('island'), the sum of the rates within the island adds up to the total number of sites within the

island:

$$\sum_{i \in \text{island}} f_i = \text{nr. of sites within the island.} \quad (17)$$

This is a consequence of conservation of probability. The span of the island may only change if a new particle is deposited within a distance $2l + 1$ from its boundary, outward from the island. This is valid in any dimension.

The larger the f_i the more probable it is that site i will receive an atom (it can come from more directions than for one with a lower f). We believe that when using the NRT, i.e., $n_r > 1$, the sites with higher f will have a higher chance to be actually deposited onto. To illustrate this, we consider the simplest setup: starting from a flat surface with a few irregularities, we perform the counting process and see with what probability the various sites will actually be deposited onto when the corresponding counters reach the threshold value n_r .

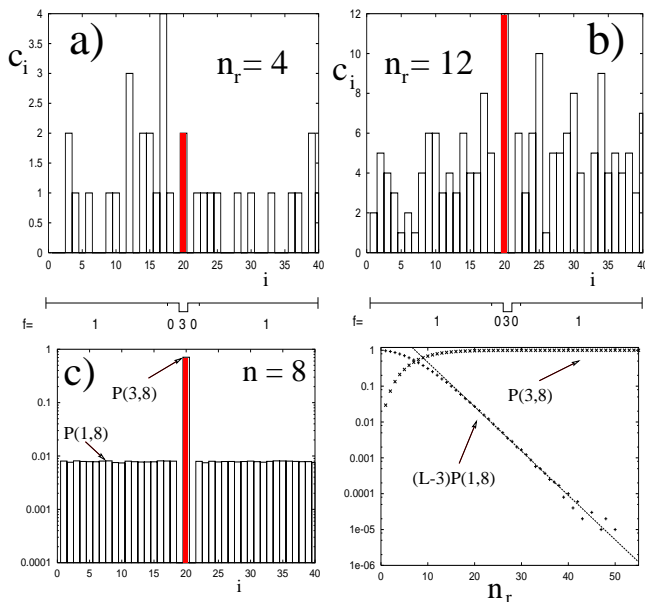


FIG. 22. Particular counter values with different noise reduction parameters a) $n_r = 4$, and b) $n_r = 12$. c) shows the probability that site i reaches the threshold for the first time. d) Plot of probability for nucleation on the terrace (of $L - 3$ sites) and deposition at the dent site with $f = 3$. The straight line is an exponential fit with slope -0.285 and intercept 8.

Unfortunately rigorous analytic derivations are difficult even in the simplest case because of the fact that surface growth is driven by the first-passage time probabilities of the counters (or waiting times). We therefore follow numerically the evolution of counters on a simple substrate which is flat everywhere except at one site where the height is lower by -1 (see the surface profile just under Fig. 22 (a)). According to both rules (WV and DT) the occupation rate is 1 except for the lower

site where it is 3 and its two nearest neighbors where it is 0. Fig. 22 (c) shows the probability that the first real deposition event occurs at site i for $n_r = 8$, $L = 40$. Obviously all sites on the flat region will have the same chance of $P(f, n_r) = P(1, n_r)$ to reach the threshold for the first time, while the site with $f = 3$ will be the most probable to reach it, and for its two nearest neighbors it is entirely unlikely: $P(0, n_r) = 0$. In case of Fig. 22 (c), $P(1, 8) = 0.0077$ and $P(3, 8) = 0.71$. This means that in spite of the uniform randomness of the shot noise, 71% of the time the actual deposition will occur on that *single* site with higher coordination and only 21% of the time we will actually be able to land an atom somewhere on the *whole flat* island of 37 sites. This clearly shows that nucleation of new islands on flat regions is strongly suppressed. In Fig. 22 (d) we represent the two probabilities $P(3, n_r)$ and $P(1, n_r)$ as functions of n_r (on a log-linear scale). For higher noise reduction parameter values we are practically forced almost each time to fill in a site with the highest occupation rate, and with almost zero probability to land an atom on the flat terrace. Looking back on Figs 17 (a) and 17 (b) for the 2+1 WV model, it becomes clear that the main particle current will be *along the step edge* (the shaded squares on the figures) and it will be greatly enhanced by NRT. At the same time the rate of island nucleation is drastically reduced, so the relaxation of the step-edge becomes rather fast compared to the creation of new islands. Since the step-edge dynamics becomes fast compared with the nucleation dynamics the mounds that are formed will grow into each other preserving their pyramidal shapes, exhibiting the observed mound-coarsening behavior. Models in 2+1 dimensions can be related to the conditional occupation rates shown in Fig. 20. The hole in the middle of the top island, and also the dents in the step-edges have much higher rates to be occupied in the WV model than in the DT model. Thus the step-edge currents are a lot stronger for the WV model than for the DT model. In addition the middle site at the base of the upper island has a lower occupation rate for the WV ($f = 2$) than for the DT ($f = 5/2 = 2.5$) model. This means that in the case of WV it is harder to disrupt a straight step-edge than for the DT model. We believe that the spectacular difference between the DT and WV noise reduced morphologies discovered in this work arise from the conditional occupation differences in the two models, which lead to an SED instability in the WV, but not in the DT model. While we have provided a rather compelling qualitative picture in this subsection explaining why the SED instability produces spectacular mounded morphologies in the NRT version ($n_r \neq 1$) of the WV model, but neither in the DT model ($n_r = 1$ or $n_r \neq 1$ version) nor in the $n_r = 1$ WV model, we have not been able to come up with an analytical theory for the mound formation, which remains an important open problem for the future.

IV. PROPERTIES OF THE MOUNDED MORPHOLOGIES

In this section, we discuss the dynamical scaling properties of the mounded morphologies presented in Section II. A conventional way [6,21] to study mounding is to look at the height-height correlation function

$$H(r) = \langle h(\mathbf{x})h(\mathbf{x} + \mathbf{r}) \rangle_{\mathbf{x}}, \quad (18)$$

where $r = |\mathbf{r}|$ is the distance between two sites on the substrate, and the $\langle \dots \rangle$ denotes a substrate averaging.

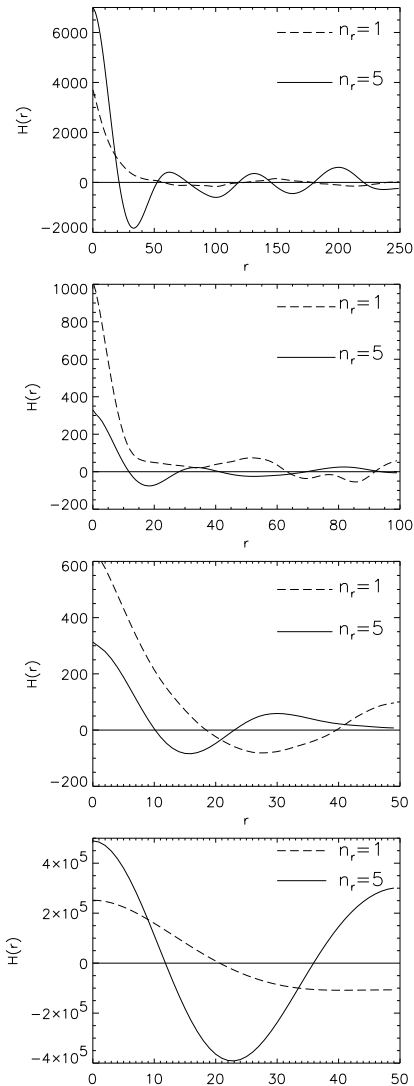


FIG. 23. The height-height correlation functions $H(r)$ corresponding to the mounded morphologies presented in Fig. 5, 8, 9, and 11. From top to bottom : the WV model at 10^4 ML, the LC model at 10^3 ML, the nonlinear fourth order at 10^3 ML, and the linear sixth order at 10^6 ML.

The calculated $H(r)$ oscillates as a function of r in systems with mounded patterns. Fig. 23 shows the oscillating correlation function from the WV, the linear fourth

order (LC model), the nonlinear fourth order, and the linear sixth order models. Note that noisy oscillations are already detectable in the original models with $n_r = 1$, but the oscillations here are weak and irregular [6]. The oscillations become spectacularly enhanced and rather evident when the noise reduction technique is used. This corroborates the fact that NRT suppresses the noise, but does not change the growth universality class.

In Fig. 24 we present the non-oscillatory $H(r)$ corresponding to the non-mounding interfaces of F, DT, and the nonlinear fourth order equation with infinite order nonlinearities (Eq. (7)) models .

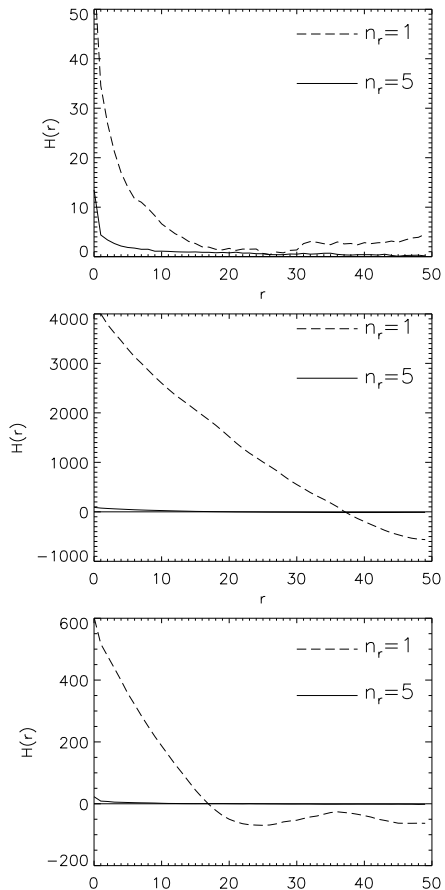


FIG. 24. The height-height correlation functions $H(r)$ corresponding to the morphologies presented in Fig. 3, 4, and 10. From top to bottom : the F model at 10^6 ML, the DT model at 10^6 ML, and the nonlinear fourth order with higher nonlinearities at 10^3 ML.

The morphologies from the original version ($n_r = 1$) of these models are kinetically rough. But when the noise is suppressed with $n_r > 1$, no specific oscillatory pattern emerges although some weak and irregular $H(r)$ oscillating could sometimes be detected in the DT model [6] (particularly for $n_r = 1$), most likely caused by the presence of the $\nabla^4 h$ Mullins term in the DT growth equation. As a matter of fact, these rough surfaces (F, DT, etc.)

merely become “smoother” and flatter for $n_r > 1$.

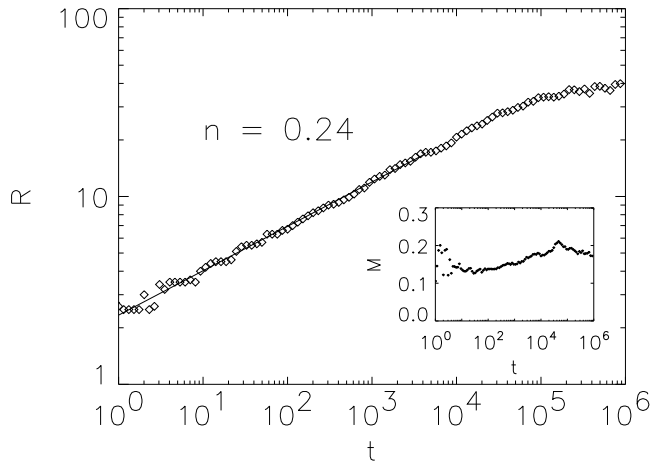


FIG. 25. The average mound radius as a function of time from the WV model with $n_r = 5$ from a substrate of size 100×100 . The average mound slope of the same system is shown in the inset

Other important characteristics of mounded patterns [6,21] are the average mound radius and the average mound slope. Conventionally, the distance of the first zero-crossing of the correlation function $H(r)$ is taken to be the average mound radius R , and $[H(r=0)]^{1/2}$ is the average mound height.

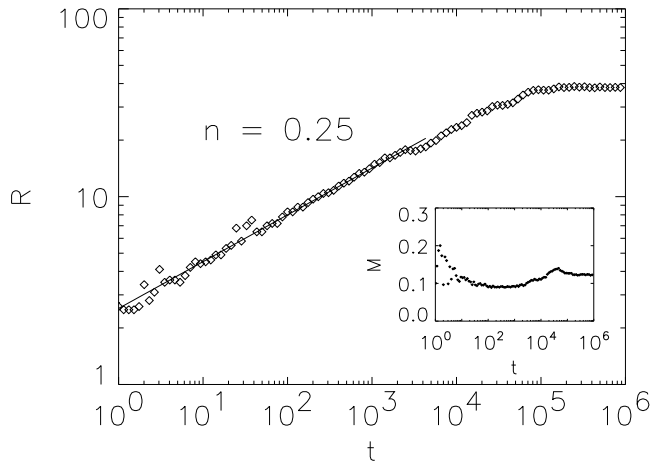


FIG. 26. The average mound radius as a function of time from the LC model with $n_r = 5$ from a substrate of size 100×100 . The average mound slope of the same system is shown in the inset

The average mound slope (M) is naturally the ratio of average mound height and average mound radius. The scaling relation for R can be written as

$$R(t) \sim t^n \quad (19)$$

where n is the *coarsening* exponent. The average mound

slope M increases in time as

$$M(t) \sim t^\lambda \quad (20)$$

where λ is the *steepening* exponent. In Fig. 25 we show the evolution of the average mound radius in the WV model with $n_r = 5$. The average mound radius is obviously increasing in time, showing that the coarsening process is dominant during the growth period with the coarsening exponent $n = 0.24$. The inset shows the average mound slope which does not change much in time ($\lambda \sim 0$).

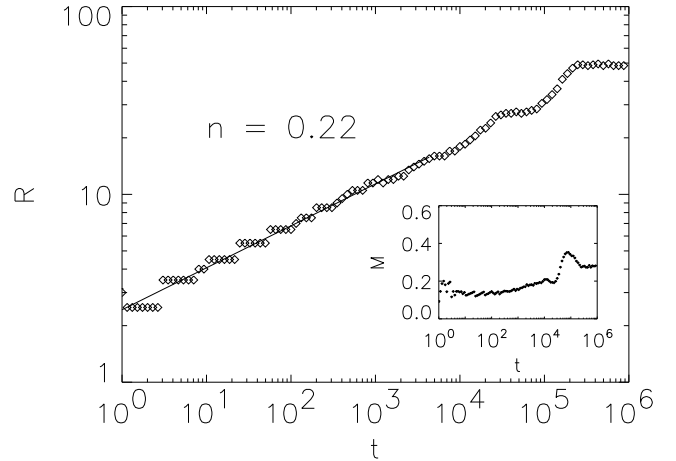


FIG. 27. The average mound radius as a function of time from the nonlinear fourth order model with $n_r = 5$ from a substrate of size 100×100 . The average mound slope of the same system is shown in the inset

This shows that the mounds in the WV model have constant magic ‘slopes’ or equivalently, the WV mounded growth exhibits slope selection. The value of this selected slope in the WV model is approximately $\tan \theta_0 \approx 0.1-0.2$ or $\theta_0 \approx 6-12^\circ$ and it does not seem to depend strongly on the value of n_r . Similar behavior is also found in the SED-induced mounded morphologies in the LC model with $n_r = 5$ (Fig. 26) and the nonlinear fourth order model with $n_r = 5$ (Fig. 27). We note that the scaling properties of the ES barrier-induced mounded morphologies are quite distinct from the SED-induced mounding instability. Asymptotically, there is no slope selection in the mound formation caused by an ES barrier [21]. After an initial crossover period, the coarsening drastically slows down with $n \rightarrow 0$ and the steepening exponent becomes exceptionally large with $\lambda \rightarrow 0.5$. Thus SED induced mounding has slope selection and ES barrier induced mounding typically does not (asymptotically).

A. Comparison with experiments

In this subsection we discuss experimental epitaxial mound formation in light of our findings about the lim-

ited mobility growth models. First and foremost we caution against the wisdom of automatically assuming the existence of an ES barrier whenever a mounded morphology is seen. As we have argued in this paper, the ES barrier is most certainly a sufficient condition to create mounded growth morphologies (nominally without any slope selection, unless some additional mechanisms, not intrinsic to ES barrier, is invoked), but by all means, it is not the *only* possible cause or a necessary condition. When analyzing experimental mounding data, therefore, an ES barrier should not be automatically assumed and more than one possibilities should be critically considered. We hope to make our point by using a recent experiment as an example [24]. It is instructive to carry out a comparison between the observed mound morphology in Cu(100) growth [24] and the mound morphology from the LC (the simple linear fourth order) model shown in this paper.

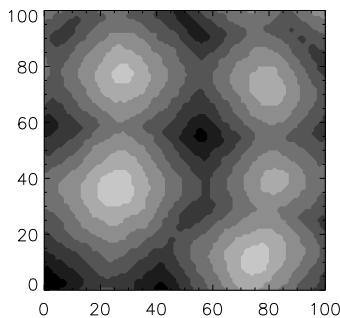


FIG. 28. The contour plot of the “equal priority” LC morphology with $l = 2$ and $n_r = 8$ at 10^4 ML.

In Fig. 28, we show a contour plot of our mounded growth front simulated from the simple LC model with diffusion length $l = 2$ and noise reduction factor $n_r = 8$. The plot looks very similar (in fact, almost identical) to the STM images of the mound morphology in reversible homoepitaxy on Cu(100) in Ref. [24]; both systems show mounds with square bases and the mounds are lined up in a somewhat regular pattern. Not only are the two systems strikingly comparable visually, but the quantitative dynamical scaling properties for the two cases are also approximately the same. In the experiment [24], the mounds have a magic slope of $5.6 \pm 1.3^\circ$ and the coarsening exponent is given as $n = 0.23 \pm 0.01$. In our LC simulation, $n \approx 0.25$ and the slope selection process is clearly observed (see Fig. 26) with typical mound slope being around 10° . The selected slopes in the two systems are not equal, but this is not particularly crucial. The LC model is only a simple dynamic growth model which in general should not be compared quantitatively with real MBE growth. We are not making a claim that there is absolutely no ES barrier effect in the Cu(100) epitaxial growth. What we want to point out here is

that the simple LC model *without* ES barrier can produce mounded morphology that is almost exactly the same as the Cu(100) mounded growth and the possibility that the mound morphology in Cu(100) may involve mechanisms other than the ES barrier should be explored. Clearly the SED mechanism as a possible source for slope selected mounding in Cu(100) growth should be taken seriously.

Finally, we recall a “puzzling” observation from Ref. [24], namely, that the *average* mound slope calculated from the ratio between the average mound height ($[H(r = 0)]^{1/2}$) and the average mound radius (first zero crossing of $H(r)$ correlation function) is much smaller than the *typical* mound slope measured from the morphology directly. In the Cu(100) case [24], the average selected slope is 2.4° and the typical mound slope is 5.6° . In our LC study, the average slope is approximately 6° while the typical slope is in the range between 10° to 15° . This is so because $[H(r = 0)]^{1/2}$ (taken as the average mound height) does not equal the typical mound height.

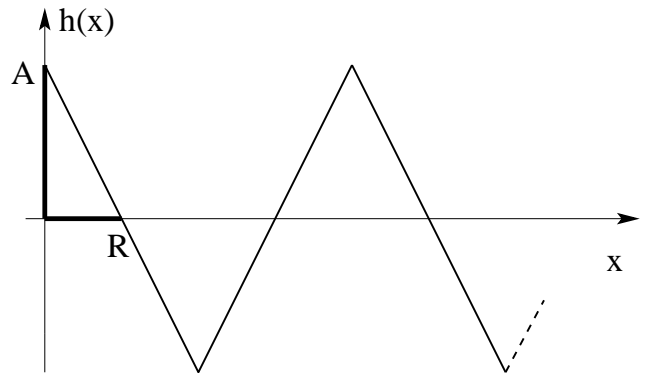


FIG. 29. A simple schematic setup to show the difference in the definitions for the average mound slope.

Let us consider the simplest “mounded” pattern which mimics the height variation in the morphology along a cut perpendicular to the base of the pyramids (see the schematic Fig. 29). In the simplest situation this is described by the periodic, piecewise linear function: $h(x) = -\frac{A}{R}(x - 4kR) + A$, if $x \in (4kR, 4k + 2R)$, and $h(x) = \frac{A}{R}(x - 4kR - 2R) - A$, if $x \in (4kR + 2R, 4k + 4R)$, $k = 0, 1, 2, \dots$, where the meaning of A and R is obvious from Fig. 29. Thus, one has for this simple shape $[H(r = 0)]^{1/2} = (A/R)/\sqrt{3} = 0.57\dots s$, where $s = A/R$ is the typical mound slope, illustrating the difference between the two definitions. In addition we also have a small discrepancy introduced by the fact that slope measured from the ratio of two averages is different from the average of the ratios. Thus, our simple LC model mounding explains another puzzling aspect of experimental mounding not easily explained via the ES barrier mechanism. We refrain from carrying out further comparison with other experimentally reported epitaxial

mounding in the literature because the main point we are making is qualitative: SED may be playing an important role in observed epitaxial mounding.

B. Global particle diffusion currents

In the *conserved* growth models where the continuity equation, Eq. (3), applies, global particle diffusion currents can be measured directly from growth on tilted substrates [25]. If the measured current is a *downhill* current (negative) then it corresponds to a *stable* surface that belongs asymptotically to the EW universality class, and an *uphill* particle current will point to an *unstable* surface (i.e. mounded morphology) [25]. Our particle current results, however, show that this concept may be misleading for growth in $d=2+1$ dimensional physical surfaces since the *global* current may show no simple systematic behavior as a function of tilt. In general, substrate current in $2+1$ dimensional growth may be positive or negative depending on tilt direction. In fact, we believe that the current measurement on tilted substrates is a useful technique for determining the universality class of growth models only in $1+1$ dimensions. In $2+1$ dimensions, where the surface current could be stabilizing in one direction (e.g. 100) and destabilizing in another (e.g. 111), the technique fails. This was not appreciated in Ref. [25] and has not been earlier discussed in the literature.

An important example is the particle current in the WV model in various dimensions. It was reported [25] that the WV model has downhill current in both one and two dimensions. This implies that the WV model belongs to the EW universality class, which was the conclusion in Ref. [25]. However, our Fig. 5 shows that the two dimensional version of the WV model has mounded morphology induced by an SED instability. This seems confusing as mound morphology should have uphill current. We repeated the particle current study on the two dimensional WV model and found the same downhill current as in the literature [25], both in the original WV model with $n_r = 1$ and in the $n_r = 5$ WV model. But all the global particle current measurements in the literature were obtained [25,26] by tilting the substrate in the (100) direction! We have also studied the diffusion current by tilting the substrate along the diagonal, i.e. in the (111) direction, and found a completely different result. The WV current from the (111) tilted substrate is *uphill* (positive). In the $n_r = 1$ model, the (111) current starts out as uphill and then crosses over to a negative value, i.e., downhill with crossover time increasing with increasing substrate size L . This is already a weak indication that there are some instabilities present. In the $n_r > 1$ WV model, however, we measure strong (111) uphill current which stays positive up to 10^6 ML which is our longest simulation time, confirming the suspicion that in fact the

WV model in two dimensions has the SED mounding instability induced by (111) uphill current, and a simple measurement of (100) downhill current gives a qualitatively incorrect result.

Our result shows that the global particle current strongly depends on how the substrate is tilted. This tilt direction (e.g. 100 versus 111) dependence may be very complicated in systems with two or higher dimensional substrates since surface current is a vectorial quantity in 2 (or higher) substrate dimensions. The particle current from one particular tilt may be highly misleading with respect to the overall behavior of the system. The downhill (100) current in the WV model had incorrectly suggested that the model belongs to the EW universality class and should exhibit relatively flat morphology in two dimensions. However, by properly suppressing the noise our study shows that the two dimensional WV model actually becomes unstable due to a strong SED driven uphill (111) current. As a matter of fact, there has been at least one prior report of mounding in the WV model in unphysical higher dimensions (three and four dimensional substrates) [27]. In higher substrate dimensions the noise effects are intrinsically a lot weaker than in one or two substrate dimensions, because diffusion in lower dimensional substrates is topologically more constrained, and therefore the SED instability is easier to observe (even without noise reduction) in higher dimensions. We have explicitly verified through direct numerical simulations that higher ($3+1$ and $4+1$) dimensional WV growth has spectacular SED instability-induced mound formation even in the absence of any noise reduction, thus verifying the old and unexplained results of Ref. [27]. The higher dimensional DT growth is smooth and flat, and exhibits no such mounding. This arises from the much stronger edge diffusion effects in higher dimensions which effectively introduces very strong intrinsic suppression of noise. Our work therefore resolves an old puzzle, explaining why the higher dimensional simulations [27] of the WV model produced mounded morphologies.

V. CONCLUSIONS

We have shown that one has to carefully account for subtle topological-kinetic instabilities when trying to understand mounding in the surface growth process. These instabilities are simply the result of the fact that in higher (higher than $1+1$) dimensions a local current may act as a stabilizing one in a certain projection on the substrate and as a destabilizing one in another projection. The local anisotropy of current effects averaged over the whole substrate may generate mounded growth even in situations (e.g. WV model) where mounding is completely unanticipated. The situations where SED instabilities may be present are rather subtle to analyze and each case has to be investigated rather carefully using the

noise reduction technique. The fact that SED mounding instability exists in the noise reduced WV, LC, and the nonlinear fourth order continuum model, but not in F, DT, and the infinite order nonlinear model shows that the kinetic-topological nature of SED mounding may not be obvious at all in a given situation. We note here that the DT model also exhibits very weak mound-like morphologies [6]. However, the weak mound-like structures in the DT model arise from the fact that the roughness exponent of the model is exceptionally large (arising from the presence of the $\nabla^4 h$ term in the growth equation). The mounds (and the oscillation in the height correlation $H(r)$) in the 2+1 DT model are random and irregular while the SED-induced mound formations (in e.g. noise reduced WV model) exhibit regular patterns with strong periodic oscillations in $H(r)$.

One of our important findings is that SED generically leads to slope-selected mounded morphology whereas the ES instability generically leads to slope steepening mounding. We believe that many of the slope selected mounding morphologies observed in MBE experiments (with typical selected slopes being small $\sim 10^\circ$ or less) may actually arise from the kinetic-topological mounding we find generically in the LC or the WV model in this paper. Further experimental and theoretical work is required to settle the competing roles of various instabilities contributing to epitaxial mounding in real surface growth.

ACKNOWLEDGMENTS

This work is supported by the NSF-DMR-MRSEC at the University of Maryland and by the US-ONR. ZT also acknowledges partial support from the DOE under contract W-7405-ENG-36 during the final stage of the manuscript preparation.

REFERENCES

-
- [1] Z. Toroczkai and E.D. Williams, Phys. Today **52**, 24 (1999).
- [2] R. L. Schwoebel, J. Appl. Phys. **40** 614 (1966); G. Ehrlich and F. G. Hudda, J. Chem. Phys. **44**, 1039 (1966).
- [3] J. G. Amar and F. Family, Phys. Rev. Lett. **77** 4584 (1996).
- [4] O. Pierre-Louis, M.R. D’Orsogna, and T.L. Einstein, Phys. Rev. Lett. **82**, 3661 (1999).
- [5] M. V. Ramana Murty and B.H. Cooper, Phys. Rev. Lett. **83**, 352 (1999) .
- [6] S. Das Sarma, P. Punyindu, and Z. Toroczkai Surf. Sci. Lett. **457**, L369 (2000).
- [7] L. Brendel, H. Kallabis, and D. E. Wolf, Phys. Rev. E, **58**, 664 (1998).
- [8] Z. W. Lai and S. Das Sarma, Phys. Rev. Lett. **66**, 2348 (1991).
- [9] F. Family, J. Phys. A **19**, L441 (1986).
- [10] S. F. Edwards and D. R. Wilkinson, Proc. R. Soc. London, Ser. A **381**, 17 (1982).
- [11] S. Das Sarma and P. I. Tamborenea, Phys. Rev. Lett. **66**, 325 (1991); P. I. Tamborenea and S. Das Sarma, Phys. Rev. E **48**, 2575 (1993).
- [12] D. Wolf and J. Villain, Europhys. Lett. **13**, 389 (1990).
- [13] J. M. Kim and S. Das Sarma, Phys. Rev. Lett. **72**, 2903 (1994).
- [14] J. Krug, Phys. Rev. Lett. **72**, 2907 (1994).
- [15] J. Villain, J. Phys. (France) I **1**, 19 (1991).
- [16] C. Dasgupta, S. Das Sarma, and J. M. Kim, Phys. Rev. E **54**, R4552 (1996); C. Dasgupta, J. M. Kim, M. Dutta, and S. Das Sarma, Phys. Rev. E **55**, 2235 (1997).
- [17] A. Kundagrami and C. Dasgupta, Physica A **270**, 135 (1999).
- [18] P. Punyindu and S. Das Sarma, Phys. Rev. E **57**, R4863 (1998).
- [19] J. Kertész and D. E. Wolf, J. Phys. A **21**, 747 (1988).
- [20] D.E. Wolf and J. Kertész, Europhys. Lett. **4**, 651 (1987).
- [21] S. Das Sarma and P. Punyindu, Surf. Sci. Lett. **424**, L339 (1999).
- [22] J. Krug, Adv.Phys. **46** 139 (1997).
- [23] W. W. Mullins, in *Metal Surfaces: Structure, Energetics and Kinetics*, eds. N.A. Gjostein and W. D. Robertson (Metals Park, Ohio: American Society of Metals, 1963). See also C. Herring, J. Appl. Phys. **21**, 301 (1950).
- [24] J.-K. Zuo and J.F. Wendelken, Phys. Rev. Lett. **78**, 2791 (1997).
- [25] J. Krug, M. Plishke and M. Siegert, Phys. Rev. Lett. **70**, 3271 (1993).
- [26] J. Krug, private communications.
- [27] M. Kotrla and P. Šmilauer, Phys. Rev. B **53**, 13777 (1996); P. Šmilauer and M. Kotrla, Europhys. Lett. **27**, 261 (1994).